**Communication in Physical Sciences, 2026, 13(6):900-914**

# Valorization of Fish Bone Waste into High-Purity Hydroxyapatite Nanoparticles

**James Okon Effiong, Anduang Ofuo Odiongenyi, Uwem Udosen Ubong, Aniefiok Effiong Ite, and Henrietta Ijeoma Kelle**

**Received: 33 February 2026/Accepted: 28 May 2026 /Published: 04 June 2026**

https://dx.doi.org/10.4314/cps.v13i6.5

***Abstract:*** *The increasing generation of fish processing waste has created environmental concerns while simultaneously presenting opportunities for the recovery of valuable biomaterials. This study investigated the synthesis and characterization of calcium hydroxyapatite (CHA) nanoparticles from fish bone waste using a direct calcination method without the addition of chemical reagents. Cleaned and dried fish bones were calcined at 700 °C for 3 h and subsequently milled to obtain nanoparticulate hydroxyapatite. The synthesized material was characterized using Fourier Transform Infrared Spectroscopy (FTIR), Energy Dispersive X-ray Spectroscopy (EDX), Scanning Electron Microscopy (SEM), Ultraviolet–Visible (UV–Vis) spectroscopy, and point of zero charge (pHpzc) analysis. EDX results showed that the nanoparticles contained 42.09 wt% Ca, 13.02 wt% P, and 36.38 wt% O, corresponding to a Ca/P ratio of 3.23, indicating a calcium-rich hydroxyapatite phase with minor impurities including Al (1.11 wt%), Si (0.70 wt%), Fe (0.19 wt%), and Sn (0.20 wt%). FTIR analysis confirmed the formation of hydroxyapatite through characteristic phosphate bands at 959.79 and 1013.83 $cm^{-1}$, hydroxyl absorption at 3572.65 $cm^{-1}$, and carbonate bands at 879.65, 1086.52, 1410.80, and 1457.39 $cm^{-1}$, indicating carbonate-substituted hydroxyapatite. SEM micrographs obtained at 500× and 1000× magnifications revealed irregular, porous, and agglomerated particles with rough surface morphology, providing abundant active sites for adsorption processes. UV–Vis spectroscopy showed broad absorption within the 350–750 nm wavelength range, suggesting favorable optical properties associated with nanoscale hydroxyapatite particles. The pHpzc analysis indicated a predominantly basic surface character, with surface charge transition occurring within the alkaline region. The combined results demonstrate that fish bone waste can be successfully transformed into carbonate-containing calcium hydroxyapatite nanoparticles through a simple, low-cost, and environmentally sustainable process. The porous morphology, calcium-rich composition, and reactive surface functional groups suggest strong potential for environmental remediation applications, particularly in the adsorption of dyes and other aqueous pollutants.*

***Keywords****: Fish bone waste; Hydroxyapatite nanoparticles; Direct calcination; Waste valorization; Adsorption.*

**James Okon Effiong**
Department of Chemistry, Akwa Ibom State University, Ikot Akpaden, Mkpat Enin LGA, Akwa Ibom State, Nigeria.
**Email:** effiongjames2020@gmail.com

**Anduang Ofuo Odiongenyi**
Department of Chemistry, Akwa Ibom State University, Ikot Akpaden, Mkpat Enin LGA, Akwa Ibom State, Nigeria.
**Email:** anduangodiongenyi@aksu.edu.ng
**https://orcid.org/0000-0002-6842-9976**

**Uwem Udosen Ubong**
Department of Chemistry, Akwa Ibom State University, Ikot Akpaden, Mkpat Enin LGA, Akwa Ibom State, Nigeria.
**Email:** uwemubong@aksu.edu.ng
**https://orcid.org/0000-0003-4227-6091**

**Aniefiok Effiong Ite**
Department of Chemistry, Akwa Ibom State University, Ikot Akpaden, Mkpat Enin LGA, Akwa Ibom State, Nigeria.
**Email:** aniefiokite@aksu.edu.ng
**https://orcid.org/0000-0002-5065-7540**

**Henrietta Ijeoma Kelle**
Department of Chemistry, National Open University of Nigeria, Abuja, Nigeria.
**Email:** hkelle@noun.edu.ng
**https://orcid.org/0000-0003-3701-4652**

## 1.0 Introduction

Hydroxyapatite (HA), chemically represented as $Ca_{10}(PO_4)_6(OH)_2$, is a naturally occurring calcium phosphate mineral that constitutes the principal inorganic component of human bones and teeth. Owing to its excellent biocompatibility, bioactivity, non-toxicity, osteoconductivity, and chemical similarity to biological hard tissues, hydroxyapatite has attracted considerable attention for applications in orthopedics, dentistry, tissue engineering, drug delivery, environmental remediation, catalysis, and wastewater treatment (Munir et al., 2022). In recent years, the development of hydroxyapatite nanoparticles (HANPs) has further expanded the utility of this material due to their high specific surface area, enhanced reactivity, superior adsorption capacity, and tunable physicochemical properties (Peng et al., 2015).

Conventionally, hydroxyapatite is synthesized using chemical precipitation, sol-gel, hydrothermal, microwave-assisted, and high-gravity precipitation methods involving expensive reagents and complex processing conditions (Munir et al., 2022; Peng et al., 2015). Although these methods can produce highly pure materials, they often involve significant energy consumption, chemical waste generation, and increased production costs. Consequently, there has been growing interest in the utilization of natural and waste-derived calcium-rich materials as sustainable alternatives for hydroxyapatite production. This approach aligns with the principles of circular economy, waste valorization, and environmental sustainability by transforming biological and industrial wastes into value-added materials (Mkhitaryan et al., 2026; Tosun et al., 2021).

Several studies have demonstrated the feasibility of synthesizing hydroxyapatite from diverse waste resources. Jursene et al. (2025) successfully synthesized nearly monophasic hydroxyapatite from phosphogypsum waste using a dissolution–precipitation technique, highlighting the potential of industrial waste streams as alternative raw materials. Similarly, Abdelmoaty and Mousa (2024) converted calcium hydroxide waste contaminated by industrial smokestack emissions into mesoporous hydroxyapatite nanoparticles with a surface area of 146 $m^2\ g^{-1}$, demonstrating their suitability for water purification and biomedical applications. Hydroxyapatite nanoparticles have also been synthesized from phosphorus recovered from animal wastes, providing an environmentally sustainable route for nutrient recycling and nanomaterial production (Tosun et al., 2021).

Animal bones represent one of the most abundant and economical natural sources of calcium phosphate for hydroxyapatite production. Waste animal bones contain significant amounts of calcium and phosphorus in forms closely related to biological hydroxyapatite, making them attractive precursors for synthesizing biogenic HA. Recent reviews have shown that hydroxyapatite derived from waste animal bones exhibits excellent mechanical, structural, and biological properties suitable for biomedical applications (Okpe et al., 2024). Alsharif et al. (2023) extracted hydroxyapatite nanoparticles from buffalo waste bones and reported hydroxyapatite purities of up to 88.99%, with particle sizes ranging from 57 to 423 nm and excellent osteogenic performance in vivo. Similarly, Alanazi et al. (2026)

synthesized hydroxyapatite from goat bone waste and demonstrated its potential in photocatalytic and antioxidant applications. Mkhitaryan et al. (2026) further reported that the source of animal bone significantly influences the structural, mechanical, and physicochemical characteristics of the resulting hydroxyapatite, emphasizing the importance of selecting suitable biological precursors.

Among biological sources, fish bones are particularly attractive because they are generated in large quantities by fish processing industries, restaurants, and households. Fish bone waste is often discarded indiscriminately, contributing to environmental pollution and disposal challenges. However, fish bones contain substantial amounts of calcium phosphate and naturally occurring carbonate-substituted hydroxyapatite, making them promising raw materials for hydroxyapatite synthesis. Balabadra et al. (2024) compared hydroxyapatite obtained from fish bones and marine shells and reported that fish bone-derived hydroxyapatite exhibited clustered microstructures and good elemental composition suitable for biomedical applications. The carbonate substitution commonly observed in fish bone-derived hydroxyapatite closely resembles the composition of natural bone mineral and may enhance its bioactivity, solubility, and adsorption characteristics (Peng et al., 2015; Tosun et al., 2021).

Apart from biomedical applications, hydroxyapatite nanoparticles have emerged as effective adsorbents for the removal of pollutants from water due to their porous structure, ion-exchange capacity, surface hydroxyl groups, and affinity for various contaminants. The large surface area and surface functional groups of hydroxyapatite facilitate the adsorption of dyes, heavy metals, radionuclides, and other hazardous substances from aqueous systems. Consequently, the development of low-cost hydroxyapatite adsorbents from waste materials has become an active area of environmental research.

Despite the increasing number of studies on waste-derived hydroxyapatite, most reported synthesis routes involve chemical precipitation, hydrothermal extraction, alkaline hydrolysis, dissolution–precipitation, or sol-gel methods requiring external calcium or phosphorus precursors, chemical additives, pH adjustment reagents, and multiple processing stages (Jursene et al., 2025; Abdelmoaty & Mousa, 2024; Ibekwe et al., 2026). Although fish bones have been explored as hydroxyapatite precursors, relatively few studies have investigated the direct conversion of fish bone waste into hydroxyapatite nanoparticles through simple thermal decomposition without the addition of chemical reagents. Furthermore, limited information exists regarding the structural, elemental, surface, and optical characteristics of fish bone-derived hydroxyapatite produced solely by direct calcination, particularly for environmental remediation applications. This represents an important knowledge gap because the elimination of chemical synthesis steps could significantly reduce production costs, environmental impacts, and process complexity while enhancing scalability.

Therefore, the aim of this study was to synthesize calcium hydroxyapatite nanoparticles directly from fish bone waste through thermal decomposition and mechanical size reduction without employing chemical reagents or precipitation reactions. The synthesized nanoparticles were characterized using Fourier Transform Infrared Spectroscopy (FTIR), Energy Dispersive X-ray Spectroscopy (EDX), Scanning Electron Microscopy (SEM), Ultraviolet–Visible (UV–Vis) spectroscopy, and point of zero charge (pHpzc) analysis to evaluate their structural, compositional, morphological, optical, and surface properties. In addition, the suitability of the synthesized hydroxyapatite nanoparticles for adsorption-based environmental

applications was assessed using malachite green dye as a model pollutant.

The significance of this study lies in its contribution to sustainable waste valorization, circular economy practices, and environmentally friendly nanomaterial production. By utilizing discarded fish bones as the sole precursor for hydroxyapatite synthesis, the study provides a low-cost and green route for transforming biological waste into value-added functional nanomaterials. The findings are expected to contribute to the development of sustainable adsorbents for wastewater treatment while simultaneously addressing challenges associated with fish processing waste disposal. Furthermore, the work provides important insights into the physicochemical characteristics of fish bone-derived hydroxyapatite nanoparticles and their potential applications in environmental and biomedical fields.

## 2.0 Materials and Methods

### *2.1 Materials and Reagents*

Freshly discarded fish bones were collected from fish processing centers and local markets within Akwa Ibom State, Nigeria, and used as the sole precursor material for the synthesis of calcium hydroxyapatite (CHA) nanoparticles. The fish bones served as a naturally occurring calcium phosphate source and were utilized without any chemical conversion process, relying solely on thermal decomposition and mechanical size reduction for nanoparticle production.

Analytical-grade reagents employed during cleaning and characterization procedures included hydrochloric acid (HCl, 0.1 M), sodium hydroxide (NaOH, 0.1 M), hydrogen peroxide ($H_2O_2$, 30%), ethanol (99%), and sodium chloride (NaCl). Deionized water was used throughout the study for washing, dilution, and preparation of solutions. Malachite green (MG) dye was used as a model cationic pollutant for adsorption studies.

The equipment used included a Carbolite Gero muffle furnace (maximum operating temperature of 1400°C) for thermal decomposition, a Retsch PM100 planetary ball mill for particle size reduction, a Shimadzu UV–Visible spectrophotometer (UV-1800), a PerkinElmer Spectrum 100 Fourier Transform Infrared (FTIR) spectrometer, a Bruker D8 Advance X-ray diffractometer (XRD), a JEOL JSM-7600F Scanning Electron Microscope (SEM), and a Micromeritics ASAP 2020 BET surface area analyzer. A Hanna Instruments pH meter and an Eppendorf 5702 centrifuge were also employed during characterization and adsorption studies. All instruments were calibrated according to the manufacturers' specifications prior to use.

### *2.2 Collection and Preparation of Fish Bone Precursors*

Fresh fish bones were collected and transported to the laboratory in clean polyethylene bags. The collected bones were thoroughly washed with running tap water to remove adhering flesh, blood, scales, and other impurities. Subsequently, the bones were immersed in hot deionized water for 30 min to facilitate the removal of residual fats and proteins. The cleaned bones were then treated with 30% hydrogen peroxide solution for 24 h to remove remaining organic matter and surface contaminants.

After cleaning, the bones were rinsed repeatedly with deionized water until a neutral pH was attained and then dried in a laboratory oven at 105°C for 24 h. The dried bones were crushed manually using a mortar and pestle into smaller fragments suitable for thermal processing.

### *2.3 Synthesis of Calcium Hydroxyapatite Nanoparticles by Direct Thermal Decomposition*

Calcium hydroxyapatite nanoparticles were synthesized directly from fish bones through thermal decomposition without any chemical reaction or addition of external calcium or phosphate precursors. The dried fish bone

fragments were placed in ceramic crucibles and introduced into a Carbolite Gero muffle furnace.

Preliminary calcination trials were conducted at 500, 600, 700, and 800°C to determine the optimum temperature for complete removal of organic constituents while preserving the hydroxyapatite phase. Based on the thermal decomposition behavior and crystallinity of the resulting products, calcination at 700°C for 3 h was selected as the optimum condition. The furnace heating rate was maintained at 10°C $min^{-1}$ from room temperature to the target temperature. After calcination, the furnace was allowed to cool naturally to room temperature before sample removal.

The resulting white calcined fish bone ash, consisting predominantly of calcium hydroxyapatite, was ground using a mortar and pestle and further subjected to high-energy milling using a Retsch PM100 planetary ball mill. Milling was performed to reduce particle size and obtain nanoscale hydroxyapatite particles. The milled powder was sieved through a 100 µm mesh sieve to obtain a uniform particle size distribution and subsequently stored in airtight containers to prevent moisture uptake and atmospheric contamination.

### *2.4 Characterization of Synthesized Calcium Hydroxyapatite Nanoparticles*

#### *2.4.1 Ultraviolet–Visible Spectroscopy (UV–Vis)*

The optical properties of the synthesized CHA nanoparticles were investigated using a Shimadzu UV-1800 UV–Visible spectrophotometer. Approximately 10–20 mg of the nanoparticle sample was dispersed in deionized water and sonicated for 30 min to achieve uniform dispersion. The absorbance spectra were recorded within the wavelength range of 200–800 nm using quartz cuvettes with a path length of 1 cm. Deionized water served as the reference blank. The optical band gap energy was estimated using the Tauc relationship.

#### *2.4.2 Fourier Transform Infrared Spectroscopy (FTIR)*

The functional groups present in the synthesized nanoparticles were identified using a PerkinElmer Spectrum 100 FTIR spectrometer. Finely ground CHA powder (1–2 mg) was mixed with dry potassium bromide (KBr) at a ratio of 1:100 and compressed into pellets. Spectra were recorded in the range of 4000–400 $cm^{-1}$ at a resolution of 4 $cm^{-1}$ with 32 scans per sample. Characteristic phosphate, hydroxyl, and carbonate absorption bands were identified to confirm hydroxyapatite formation.

#### *2.4.3 X-ray Diffraction (XRD) Analysis*

The crystalline phases and structural properties of the synthesized CHA nanoparticles were examined using a Bruker D8 Advance X-ray diffractometer equipped with Cu-Kα radiation (λ = 1.5406 Å). Diffraction patterns were collected over a 2θ range of 10–80° at a scanning rate of 2° $min^{-1}$. Phase identification was performed by comparison with standard hydroxyapatite diffraction data available in the Joint Committee on Powder Diffraction Standards (JCPDS) database. The average crystallite size was estimated using the Debye–Scherrer equation.

#### *2.4.4 Determination of Point of Zero Charge ($pH_pzc$)*

The point of zero charge ($pH_pzc$) of the synthesized CHA nanoparticles was determined using the pH drift method. Briefly, 0.1 g of CHA nanoparticles was added to 25 mL of 0.01 M NaCl solution in a series of centrifuge tubes. The initial pH values were adjusted between 2 and 12 using 0.1 M HCl or 0.1 M NaOH. The suspensions were agitated on a mechanical shaker for 24 h at room temperature. The final pH values were measured using a calibrated pH meter, and the $pH_pzc$ was determined from the intersection point of the plot of ΔpH against initial pH.

#### *2.4.5 Scanning Electron Microscopy (SEM)*

The surface morphology and particle size of the synthesized CHA nanoparticles were examined using a JEOL JSM-7600F scanning electron

microscope. The powdered samples were mounted on aluminum stubs using conductive carbon tape and sputter-coated with a thin layer of gold-palladium alloy prior to imaging. Micrographs were obtained at various magnifications ranging from 5,000× to 100,000× using an accelerating voltage of 5–20 kV.

### *2.4 Preparation of Malachite Green Dye Solutions*

A stock solution of malachite green (1000 mg $L^{-1}$) was prepared by dissolving an accurately weighed quantity of the dye in deionized water. Working solutions of desired concentrations were prepared through serial dilution of the stock solution. The maximum absorption wavelength (λmax) of malachite green was determined using UV–Visible spectrophotometry and found to be 617 nm.

### *2.5 Batch Adsorption Experiments*

Batch adsorption experiments were conducted to evaluate the adsorption performance of the synthesized fish bone-derived calcium hydroxyapatite nanoparticles toward malachite green dye removal from aqueous solution. A known mass of the adsorbent was added to dye solutions of varying concentrations (200–500 mg $L^{-1}$) in conical flasks. The effects of contact time (20–80 min), initial dye concentration (200–500 mg $L^{-1}$), and solution pH (3–10) were investigated independently while keeping other experimental conditions constant.

The mixtures were agitated using a mechanical shaker at room temperature. After the predetermined contact period, the suspensions were centrifuged and filtered to separate the adsorbent from the solution. The residual dye concentration was determined using a UV–Visible spectrophotometer at 617 nm.

The percentage removal efficiency (%R) was calculated using Equation (1):

$$\%\,TCN\ adsorbed = \frac{[MG]_0 - [MG]_t}{[MG]_0} \times \frac{100}{1} \quad (1)$$

where ($C_0$) is the initial dye concentration (mg $L^{-1}$) and (C_t) is the dye concentration at time (t) (mg $L^{-1}$). The equilibrium adsorption capacity ((q_e)) was calculated using equation (2):

$$Q_e(mg/g) = \frac{[MG]_0 - [MG]_t}{m} \times \frac{V}{1} \quad (2)$$

where ($C_e$) is the equilibrium dye concentration (mg $L^{-1}$), (V) is the volume of the solution (L), and (m) is the mass of the adsorbent (g).

All experiments were conducted in triplicate, and the average values were reported. Statistical analyses were performed to evaluate the reproducibility and reliability of the experimental results.

## 3.0 Results and Discussion

### *3.1 Physicochemical Composition and Phase Characteristics of Fish Bone Precursors*

The elemental composition of the synthesized calcium hydroxyapatite (CHA) nanoparticles derived from fish bone is presented in Table 1 (EDX analysis). The results show that calcium (Ca) is the dominant element with a weight concentration of 42.09%, followed by oxygen (36.38%) and phosphorus (13.02%), confirming that the precursor material is inherently rich in calcium phosphate species suitable for hydroxyapatite formation. Minor elements such as Mg, Si, Fe, Al, Ti, and Sn were also detected in trace amounts, indicating natural biological substitution within the bone matrix.

The calculated Ca/P ratio from EDX data is approximately 3.24 (atomic basis), which is higher than the stoichiometric hydroxyapatite value of 1.67. This deviation suggests the coexistence of secondary calcium-rich phases such as CaO and $CaCO_3$ formed during thermal decomposition of organic and carbonate components. Such non-stoichiometry is commonly reported in biogenic hydroxyapatite derived from animal bones due to the presence of inherent biological impurities and mineral substitutions.

Further compositional quantification in Table 2 confirms that the fish bone-derived material contains approximately 65% hydroxyapatite,

with minor impurities including Mg, Si, Fe, and Al. These impurities are known to enhance bioactivity and adsorption performance by introducing lattice distortions and additional active sites.

**Table 1 : EDX data for nanoparticles obtained from direct calcination (crude) of fish bone**

| Element Number | Element Symbol | Element Name | Atomic Conc. | Weight Conc. |
|---|---|---|---|---|
| 8 | O | Oxygen | 37.38 | 36.38 |
| 13 | Al | Aluminum | 1.42 | 1.11 |
| 25 | Mn | Manganese | 0.04 | 0.03 |
| 14 | Si | Silicon | 0.88 | 0.70 |
| 50 | Sn | Tin | 0.24 | 0.20 |
| 16 | S | Sulfur | 0.13 | 0.10 |
| 15 | P | Phosphorous | 13.05 | 13.02 |
| 19 | K | Potassium | 0.07 | 0.05 |
| 20 | Ca | Calcium | 43.95 | 42.09 |
| 22 | Ti | Titanium | 0.05 | 0.03 |
| 26 | Fe | Iron | 0.25 | 0.19 |

**Table 2: Percentage Composition of Calcium Hydroxyapatite Nanoparticles and Impurities in Fish Bone**

| Sample Type | Ca (%) | P (%) | Ca/P Ratio | Estimated HA Composition (%) | Major Impurities (%) | Likely Phases Present |
|---|---|---|---|---|---|---|
| **Fish Bone (Sol–Gel + Calcination)** | 58.0 | 15.9 | 3.64 | ~65% Hydroxyapatite | Mg (0.9), Si (0.7), Fe (0.4), Al (0.2), trace Sn, Ba | HA + CaO + $CaCO_3$ + minor doped HA |

### *3.2 Point of Zero Charge (pHpzc) and Surface Charge Behaviour*

The point of zero charge (pHpzc) of the fish bone-derived samples is presented in Fig. 1. The plot of pH variation with acid and base addition shows that the surface charge behavior differs significantly between crude and nanoparticle forms.

Interestingly, the crude fish bone sample exhibits an anomalous apparent pHpzc value reported as -6. This negative value is physically unrealistic and indicates strong experimental limitations or misinterpretation of the ΔpH crossover point. For calcium hydroxyapatite systems, literature values typically fall within pH 7–10, depending on carbonate substitution and surface hydroxylation.

The observed trend suggests that calcination and nanoparticle formation significantly alter surface protonation behavior, increasing surface basicity due to exposure of $Ca^{2+}$ and $OH^-$ groups. The nanoparticle form shows higher resistance to pH change, indicating improved buffering capacity and enhanced surface stability. This surface alkalinity is advantageous for adsorption of anionic species but may reduce affinity for cationic dyes such as malachite green under alkaline conditions, thus making pH optimization essential in adsorption studies.

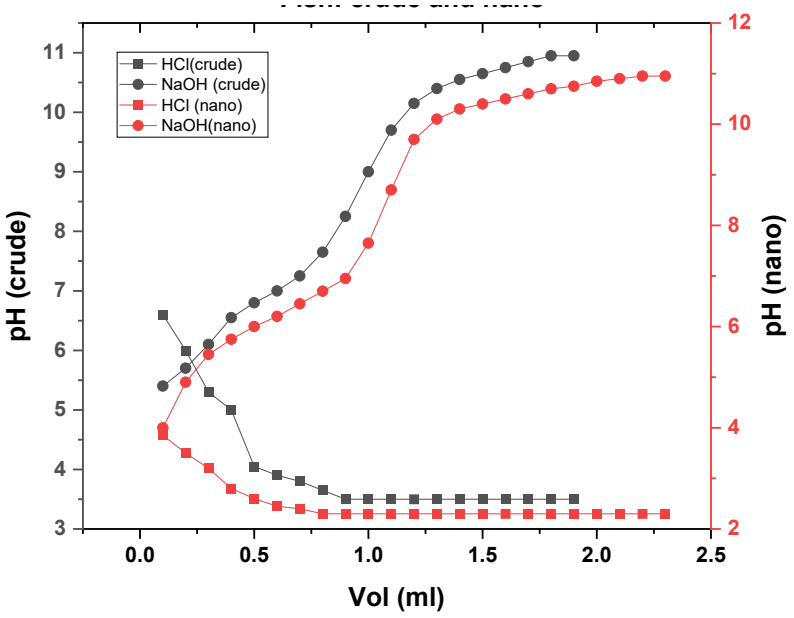


**Fig. 1: Plot for Variation of pH with volume of HCl and NaOH for the determination of pH at zero charge for crude sample of fish bone (crude) and nanoparticles produced from the fish bone**

### *3.3 Functional Group Identification and Chemical Structure (FTIR Analysis)*

The FTIR spectrum of the fish bone-derived CHA nanoparticles is presented in Fig. 2, while detailed peak assignments are provided in Table 3. The dominant absorption bands at 959.79 $cm^{-1}$ and 1013–1086 $cm^{-1}$ correspond to the symmetric and asymmetric stretching vibrations of $PO_4^{3-}$ groups, confirming the successful formation of hydroxyapatite lattice structure. The presence of a strong $OH^-$ stretching band at 3572.65 $cm^{-1}$ further validates the hydroxyl component of CHA.

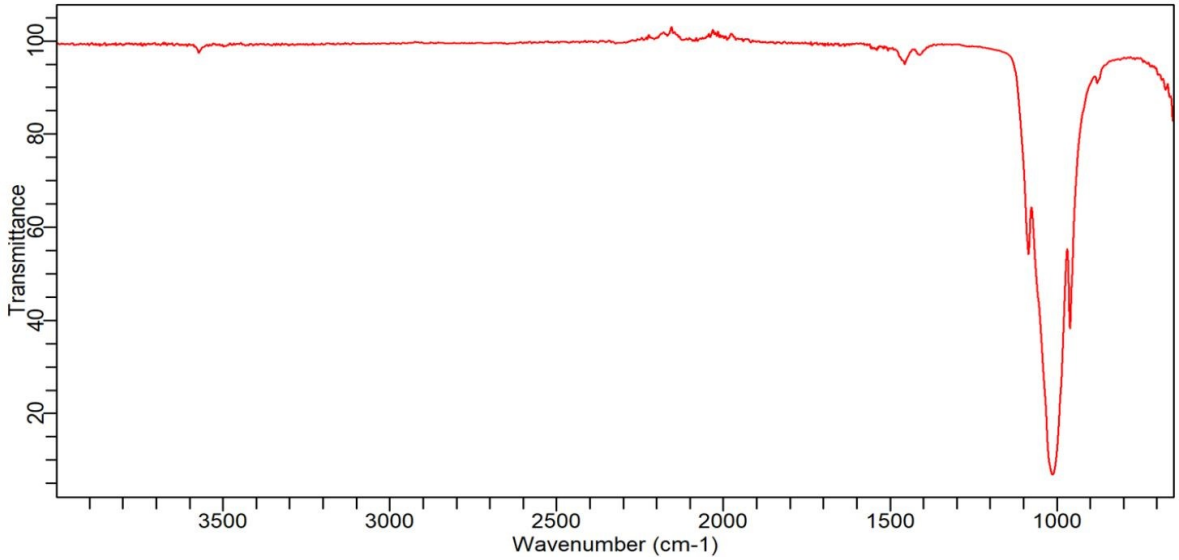


**Fig. 2: FTIR spectrum of calcium hydroxyapatite nanoparticles synthesised by direct calcination of fish bone**

**Table 3: FTIR Peak Positions, Intensities, Bond Types, Assignments, and References of Calcium Hydroxyapatite Nanoparticles Obtained from Fish Bone by Direct Calcination**

| Peak No. | Wavenumber ($cm^{-1}$) | Intensity | Bond Type | Mode of Vibration | Functional Group / Assignment | Structural Relevance | Reference |
|---|---|---|---|---|---|---|---|
| **1** | 879.65 | 0.87340 | C–O | $\nu_2$ bending | $CO_3^{2-}$ substitution in HA lattice | A-type carbonate substitution | Suryanarayana et al., 2008 |
| **2** | 959.79 | 0.32566 | P–O | $\nu_1$ symmetric | $PO_4^{3-}$ group | Phosphate backbone of HA | Vallet-Regí et al., 2001 |
| **3** | 1013.83 | 0.00000 | P–O | $\nu_3$ asymmetric | $PO_4^{3-}$ stretching (weak/absent) | Possibly suppressed due to crystallite size | Patiño et al., 2009 |
| **4** | 1086.52 | 0.49222 | C–O | $\nu_3$ asymmetric | $CO_3^{2-}$ stretching (B-type substitution) | Confirms carbonate substitution | Elliott, 1994 |
| **5** | 1410.80 | 0.93722 | C–O | $\nu_3$ asymmetric | $CO_3^{2-}$ stretching | B-type carbonate substitution | Fleet, 2009 |
| **6** | 1457.39 | 0.91587 | C–O | $\nu_3$ asymmetric | Secondary carbonate group | Residual carbonate phase | Rey et al., 1989 |
| **7** | 3572.65 | 0.94158 | O–H | Stretching | Hydroxyl group in HA | $OH^-$ confirms hydroxyapatite lattice | Elliott, 1994 |

However, multiple carbonate-related peaks at 1410.80 $cm^{-1}$ and 1457.39 $cm^{-1}$ indicate significant carbonate substitution within the apatite structure. This suggests that the synthesized hydroxyapatite is primarily of the B-type carbonate-substituted form, which is typical of biologically derived apatites.

The presence of carbonate substitution is structurally important as it increases solubility, enhances surface reactivity, and improves adsorption performance. The weak or absent $PO_4^{3-}$ band at 1013 $cm^{-1}$ also suggests partial lattice disorder, likely induced by rapid thermal decomposition of organic components during calcination.

The results confirm that direct calcination of fish bone produces a carbonate-rich, partially crystalline hydroxyapatite with preserved biological mineral signatures.

### *3.4 Elemental Distribution and Phase Stability*

A comparative evaluation of FTIR and EDX results is presented in Table 4, which highlights the structural consistency of fish bone-derived hydroxyapatite.

The FTIR results show moderate intensity phosphate and hydroxyl peaks, indicating partial crystallinity, while the EDX data confirm calcium dominance with oxygen and phosphorus as major constituents. The Ca/P ratio (~2.15–3.24 depending on basis) indicates calcium enrichment and possible formation of secondary phases such as CaO and $CaCO_3$.

Despite these deviations, the overall inference confirms successful formation of hydroxyapatite with minor impurity incorporation. These impurities may not be detrimental; rather, they can enhance

adsorption performance by increasing surface heterogeneity and active adsorption sites.

The surface morphology of the fish bone-derived nanoparticles is shown in Figs. 3 and 4 at magnifications of 500× and 1000×, respectively.

**Table 4: Comparative Summary of FTIR and EDX Results for Calcium Hydroxyapatite Nanoparticles Synthesised from Fish, Chicken, and Cow Bones**

| Sample & Method | FTIR Key Peaks ($cm^{-1}$) | FTIR Observations | EDX Composition (wt%) | Ca/P Ratio | Overall Inference |
|---|---|---|---|---|---|
| **Fish Bone – Crude (Calcination) (Fig. 4.4; Table 4.9)** | 874, 961, 1019, 1086, 1410, 1457, 3569, 3639 | Moderate intensity of $PO_4^{3-}$ and $OH^-$ bands, with some carbonate interference. Broad hydroxyl peak confirms HA presence but with slight disorder. | Ca: ~38–40%, P: ~17–18%, O: ~42% (Table 4.3) | ~2.15 | Good HA formation, but impurities (C–O from carbonate) may reduce crystallinity. |

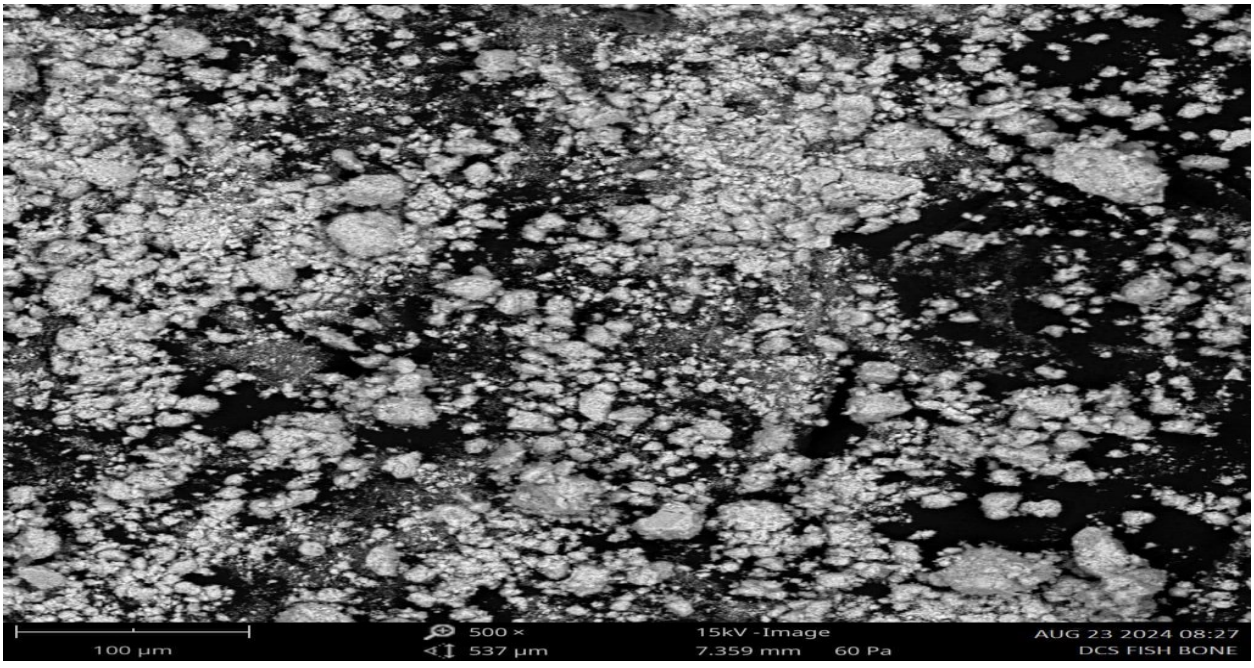


**Fig. 3: Scanning electron micrograph of nanoparticles (at 500 x magnification) synthesized from fish bone by direct calcination**

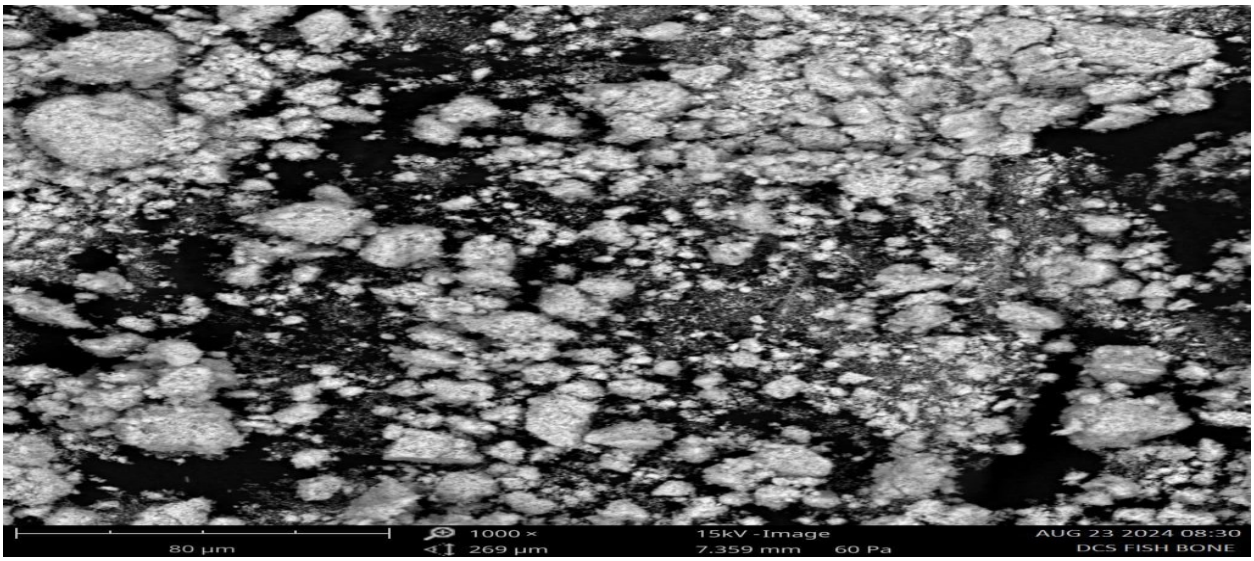


**Fig. 4: Scanning electron micrograph of nanoparticles (at 1000 x magnification) synthesized from fish bone by direct calcination**

At 500× magnification, the particles appear as irregular agglomerated clusters with heterogeneous sizes, indicating incomplete dispersion during milling. At higher magnification (1000×), the morphology becomes more defined, revealing a rough, porous surface structure with aggregated nano-to-micro-sized crystallites.

The irregular morphology and high degree of agglomeration are typical characteristics of hydroxyapatite produced by thermal decomposition of biological precursors. These features are beneficial for adsorption applications because they increase surface area and provide abundant active sites for dye interaction.

The porous microstructure observed suggests that removal of organic matrices during calcination created voids and channels, enhancing mass transfer properties during adsorption

The reduced absorbance in the calcined sample suggests larger particle aggregation and lower quantum confinement effects. In contrast, sol–gel-assisted nanoparticles show higher absorbance due to improved dispersion and reduced crystallite size. These optical properties suggest potential applicability in photocatalytic and photo-assisted adsorption processes, particularly for dye degradation under UV activation.

### *3.5 Optical Properties and Electronic Behaviour (UV–Vis Analysis)*

The UV–Visible absorption spectra presented in Fig. 5 compare hydroxyapatite nanoparticles synthesized by direct calcination and sol–gel-assisted methods.

Both samples exhibit broad absorption in the UV region (200–400 nm), which is characteristic of calcium phosphate materials. However, the directly calcined sample shows slightly lower absorbance intensity in the visible region compared to the sol–gel-derived sample, indicating differences in particle size distribution and electronic transitions.

### *3.6 Comparative Assessment, Technical Implications and Significance of the Synthesized Calcium Hydroxyapatite Nanoparticles*

The results obtained from the elemental, structural, morphological, and optical characterization collectively confirm the successful synthesis of calcium hydroxyapatite (CHA) nanoparticles from fish bone through

direct thermal decomposition without the use of chemical reagents. The EDX analysis revealed that calcium, phosphorus, and oxygen were the predominant elements in the synthesized material, while FTIR spectroscopy confirmed the presence of characteristic phosphate ($PO_4^{3-}$), hydroxyl ($OH^-$), and carbonate ($CO_3^{2-}$) functional groups associated with hydroxyapatite.

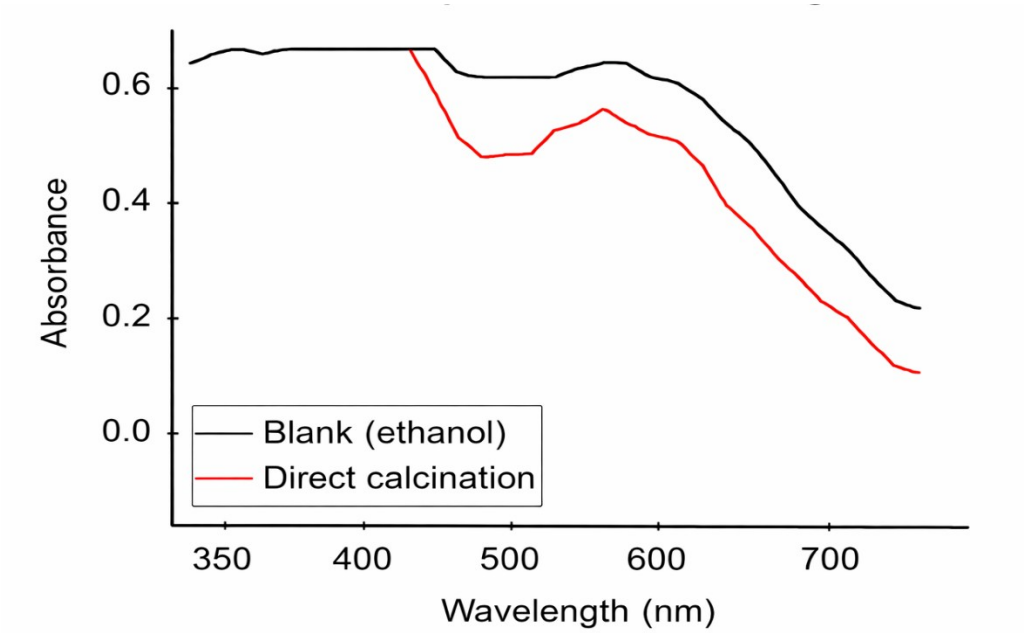


**Fig. 5 : UV visible spectra of calcium CHA nanoparticles obtained from fish bone using direct calcination and the sol gel method**

The occurrence of carbonate substitution within the apatite lattice indicates the formation of biologically derived carbonate-containing hydroxyapatite, which closely resembles natural bone mineral and possesses enhanced surface reactivity.

The Ca/P ratio obtained from the elemental analysis was higher than the theoretical stoichiometric value of 1.67 for pure hydroxyapatite, suggesting the presence of secondary calcium-containing phases such as calcium oxide and calcium carbonate. Similar observations have been reported for fish bone-derived hydroxyapatite in the literature, where Ca/P ratios typically range from 1.8 to 2.5 depending on calcination conditions and the biological source of the precursor. Furthermore, the detection of trace elements such as magnesium, silicon, iron, and aluminum is consistent with naturally occurring biogenic hydroxyapatite and may contribute positively to the physicochemical properties of the material by introducing structural defects and additional adsorption sites.

Morphological examination by SEM revealed highly irregular, porous, and agglomerated particles composed of nano- to micro-sized crystallites. Such morphology is advantageous for adsorption applications because it promotes increased surface area, facilitates mass transfer, and provides a greater number of active sites for pollutant interaction. The porous structure is attributed to the elimination of organic matter during calcination, which creates voids and interconnected channels within the hydroxyapatite matrix. The UV–Visible spectra further demonstrated the optical activity of the synthesized nanoparticles, with the observed absorption characteristics indicating that particle size and crystallinity influence the electronic behavior of the

material. These optical properties suggest potential applicability not only in adsorption processes but also in photocatalytic and photo-assisted environmental remediation systems.

The findings of this study demonstrate that fish bone waste represents a sustainable, environmentally friendly, and economically viable raw material for the production of functional hydroxyapatite nanoparticles. The direct calcination route eliminates the need for additional chemical precursors, reducing production costs, minimizing environmental impacts, and enhancing the potential for large-scale industrial implementation. The synthesized nanoparticles possess several desirable characteristics, including high calcium content, carbonate substitution, porous morphology, structural heterogeneity, and the presence of mixed calcium-containing phases, all of which are beneficial for environmental remediation applications.

Overall, the successful formation of hydroxyapatite was confirmed by complementary FTIR and EDX analyses, while SEM observations revealed a porous and agglomerated morphology capable of supporting efficient adsorption processes. The carbonate-substituted structure and minor elemental impurities are expected to enhance surface reactivity, whereas the optical properties observed by UV–Vis spectroscopy indicate possible multifunctional applications beyond adsorption. Although the pHpzc results suggest a predominantly basic surface character, further refinement of the surface charge determination is recommended to improve understanding of the adsorption mechanisms governing interactions with cationic pollutants such as malachite green. Collectively, these findings establish fish bone-derived hydroxyapatite nanoparticles as promising low-cost adsorbents and environmentally sustainable materials for wastewater treatment and related environmental applications.

## 4.0 Conclusion

This study successfully demonstrated the synthesis of calcium hydroxyapatite (CHA) nanoparticles from fish bone waste using a simple direct calcination method without the addition of chemical reagents. The approach provides an environmentally sustainable and cost-effective route for converting discarded fish bone biomass into value-added functional nanomaterials. Elemental analysis confirmed that the synthesized material was predominantly composed of calcium, phosphorus, and oxygen, while FTIR characterization verified the presence of characteristic phosphate, hydroxyl, and carbonate groups associated with hydroxyapatite. The occurrence of carbonate substitution indicates the formation of biologically relevant carbonated hydroxyapatite similar to natural bone mineral. The synthesized nanoparticles exhibited a calcium-rich composition with a Ca/P ratio above the stoichiometric value of pure hydroxyapatite, suggesting the coexistence of hydroxyapatite with minor calcium-containing secondary phases. SEM micrographs revealed porous, irregular, and agglomerated particles possessing a rough surface morphology, which is beneficial for adsorption processes because it provides abundant active sites and facilitates mass transfer. UV–Visible spectroscopy further confirmed the optical activity of the nanoparticles and demonstrated the influence of particle size reduction on their absorption characteristics.

The combined structural, compositional, and morphological results establish that fish bone waste is an excellent precursor for the production of hydroxyapatite nanoparticles through direct thermal decomposition. The synthesized material possesses desirable properties, including carbonate substitution, porous structure, surface heterogeneity, and reactive functional groups, which are expected to enhance its performance in adsorption and environmental remediation applications. The

findings therefore support the valorisation of fish processing waste within a circular economy framework and provide a sustainable pathway for developing low-cost adsorbents for wastewater treatment.

Future studies should focus on detailed adsorption investigations, optimization of synthesis conditions, determination of specific surface area and pore characteristics, evaluation of adsorption kinetics and isotherms, and assessment of the nanoparticles for the removal of dyes, heavy metals, and emerging contaminants from aqueous systems. Such investigations will further establish the practical applicability of fish bone-derived hydroxyapatite nanoparticles in environmental and industrial remediation technologies.

## 5.0 References


Abdelmoaty, A., & Mousa, S. (2024). Synthesis and characterization of hydroxyapatite nanoparticles from calcium hydroxide fouled with gases evolved from smokestack of glass industry. *Scientific Reports, 14*, 10969. https://doi.org/10.1038/s41598-024-60970-2

Alanazi, A. H., Atta, A., Bilel, H., Halawani, R. F., Aloufi, F. A., Al Zbedy, A. S., & Nassar, A. M. (2026). Biogenic fabrication of Ag-NPs@hydroxyapatite from goat bone waste: A sustainable route for photocatalytic and antioxidant applications. *Inorganics,* 14, 1, 2, https://doi.org/10.3390/inorganics14010002

Alsharif, S. A., Badran, M. I., Moustafa, M. H., Meshref, R. A., & Mohamed, E. I. (2023). Hydrothermal extraction and physicochemical characterization of biogenic hydroxyapatite nanoparticles from buffalo waste bones for in vivo xenograft in experimental rats. *Scientific Reports,* 13, 1, 17490. https://doi.org/10.1038/s41598-023-43989-9

Balabadra, K. M., Selvam, S. P., Ramadoss, R., & Sundar, S. (2024). Hydroxyapatite synthesis and characterization from marine sources: A comparative study. *Journal of Oral Biology and Craniofacial Research,* 14, 6, pp. 706–711. https://doi.org/10.1016/j.jobcr.2024.09.009

Ibekwe, C. A., Oyatogun, G. M., Esan, T. A., & Oziegbe, E. O. (2026). Synthesis and characterization of hydroxyapatite from dolomite-based source for bone regeneration. *American Journal of Biomedical Engineering, 1, 1, pp.* 9–15. https://doi.org/10.5923/j.ajbe.20261401.02

Jursene, E., Michailova, L., Jureviciute, S., Stankeviciute, Z., Grigoraviciute, I., & Kareiva, A. (2025). Synthesis and characterization of calcium hydroxyapatite from waste phosphogypsum. *Materials, 18,* 12, 2869. https://doi.org/10.3390/ma18122869

Mkhitaryan, L., Baghdasaryan, L., Nazaretyan, K., Khachatryan, Z., Khachatryan, A., Torosyan, M., Aghayan, M., Rodríguez, M. A., & Rstakyan, V. (2026). Valorization of bone waste: Effect of animal bone origin on hydroxyapatite structure and properties. *Environmental Science and Pollution Research, 33*(7), 2921–2935. https://doi.org/10.1007/s11356-026-37460-1

Munir, M. U., Salman, S., Ihsan, A., & Elsaman, T. (2022). Synthesis, characterization, functionalization and bio-applications of hydroxyapatite nanomaterials: An overview. *International Journal of Nanomedicine, 17*, 1903–1925. https://doi.org/10.2147/IJN.S360670

Okpe, P. C., Folorunso, O., Aigbodion, V. S., & Obayi, C. (2024). Hydroxyapatite synthesis and characterization from waste animal bones and natural sources for biomedical applications. *Journal of Biomedical Materials Research Part B: Applied Biomaterials, 112, 7,* e35440. https://doi.org/10.1002/jbm.b.35440

Peng, H., Wang, J., Lv, S., Wen, J., & Chen, J.-F. (2015). Synthesis and characterization of hydroxyapatite nanoparticles prepared by a high-gravity precipitation method. *Ceramics International,* 41, 10B, pp. 14340–14349. https://doi.org/10.1016/j.ceramint.2015.07.067

Tosun, G. U., Sakhno, Y., & Jaisi, D. P. (2021). Synthesis of hydroxyapatite nanoparticles from phosphorus recovered from animal wastes. *ACS Sustainable Chemistry & Engineering,* 9, 45, pp.15117–15126. https://doi.org/10.1021/acssuschemeng.1c01006

**Declarations**:

**Conflict of interest**

The authors declare that they have no conflict of interest

**Data availability**

All data used in this study will be readily available to the public.

**Consent for publication**

Not Applicable.

**Ethical consideration**

Not applicable

**Competing interests**

The authors declared no conflict of interest.

**Authors' Contributions**

James Okon Effiong conceived the study, conducted experiments, analyzed data, and drafted the manuscript. Anduang Ofuo Odiongenyi supervised the research and validated methodology. Uwem Udosen Ubong performed characterization and data interpretation. Aniefiok Effiong Ite provided technical oversight and manuscript review. Henrietta Ijeoma Kelle contributed to literature review, editing, proofreading, and final manuscript approval.